ADVANCED OPTICAL MATERIALS
www.advopticalmat.de

Colored, Daytime Radiative Coolers with Thin-Film Resonators for Aesthetic Purposes

*Gil Ju Lee, Yeong Jae Kim, Hyun Myung Kim, Young Jin Yoo, and Young Min Song**

Recently developed approaches in passive radiative cooling enable daytime cooling via engineered photonic structure layouts. However, the use of these daytime radiative coolers is restricted owing to their nonaesthetic appearance resulted from strong solar reflection. Therefore, this article introduces a colored passive radiative cooler (CPRC) capable of generating potential cooling power, based on a thin-film optical resonator embedded in an efficient thermal emission structure. This CPRC not only selectively emits infrared wave through the atmospheric transparency window but also displays subtractive primary colors to exhibit the desired appearance. Theoretical analysis and systematic experiments prove the possibility of subambient cooling via CPRC by lowering the temperature to 3.9 °C below the ambient air in the daylight. This is the first example of coloring radiative cooler by photonic structures. Successful demonstration of cooling/coloring behavior with wearable electronic devices under solar irradiation represents a major step forward in the field of temperature-sensitive, flexible, wearable electronic/optoelectronic devices.

Passive cooling requires no electricity and thus provides opportunities to solve problems associated with the energy crisis.[1–4] Recently developed concepts in photonic designs, nanomaterials, and manufacturing approaches have opened up the possibilities for passive radiative coolers that function in the daytime, which can afford exceptional levels of energy savings.[5–13] Efficient radiative cooling is achieved by using selective emitters (SE) that effectively radiate heat to outer space through the atmospheric transparency window (i.e., 8–13 μm). In addition, for daytime cooling, high reflectivity in the entire solar spectral range (i.e., 300–4000 nm) is required to minimize heat generation from the absorbed solar power. Potential applications of these daytime coolers include temperature-sensitive electronic/optoelectronic devices such as photovoltaics,[14–17] thermophotovoltaics,[18–20] rectennas,[21] infrared detectors,[22] and power electronics[23–25] not limited to buildings and power plants.

An overarching goal in the development of daytime radiative coolers is to achieve enhanced net cooling power under direct sunlight. The features of an accurate radiative model, strong selective emission in the atmospheric transparency window, and broadband high reflectance to solar irradiation are each formulated individually and then configured collectively to accomplish this outcome. Because all of the successful examples of daytime radiative coolers possess high solar reflectivity, they are white or silver in color and are thus not visually appealing,[5–7,9] thereby restricting the possible installation locations and limiting their net cooling capacity. Although previous efforts have been paid to incorporate colors into the radiative cooler,[26] the research only dealt with theoretical calculations without experimental demonstrations, and structural optimization of colored radiative coolers has not been performed. Here, we present concepts and strategies for daytime radiative cooling systems that involve comparable attention to engineering design but with the goal of achieving systems that offer aesthetically desired colors and patterns and functional purposes, thus enabling more widespread installation. The experimental demonstration exhibits subambient cooling behaviors under a clear sky while preserving its color. The approaches reported here can address application concepts for wearable electronic devices whose operational temperature is lowered by radiative cooling.

Figure 1a exhibits a schematic of a decorative colored passive radiative cooler (CPRC) for aesthetic purposes featuring areas with subtractive primary colors (i.e., cyan, magenta, and yellow) on a silvery background, where the latter area represents a conventional daytime radiative cooler. The CPRC consists of a SE comprising a bilayer of SiO_2 (650 nm) and Si_3N_4 (910 nm), whose thicknesses are defined by extensive numerical optimization; and a metal reflector comprising an Ag film (100 nm) deposited on a silicon substrate (Figure 1b, left). Additional photonic nanostructures were inserted below the SE to generate vivid colors at specific desired areas (Figure 1b, right), which comprised a thin-film resonator composed of a metal–insulator–metal (MIM) structure. The MIM structure determined each color via interference in the 1D stacked layers, where the color generation was precisely controlled by tuning the thickness of the insulator layer (i.e., SiO_2 cavity) in the MIM.

In this study, the MIM structure was chosen as the colorant structure because it provided minimal loss of solar reflectance and a narrow spectral width compared with other additive color filters such as metal gratings and 1D photonic crystals (1D PhC),

G. J. Lee, Y. J. Kim, H. M. Kim, Y. J. Yoo, Prof. Y. M. Song
School of Electrical Engineering and Computer Science (EECS)
Gwangju Institute of Science and Technology (GIST)
Gwangju 61005, Republic of Korea
E-mail: ymsong@gist.ac.kr
The ORCID identification number(s) for the author(s) of this article can be found under https://doi.org/10.1002/adom.201800707.

DOI: 10.1002/adom.201800707

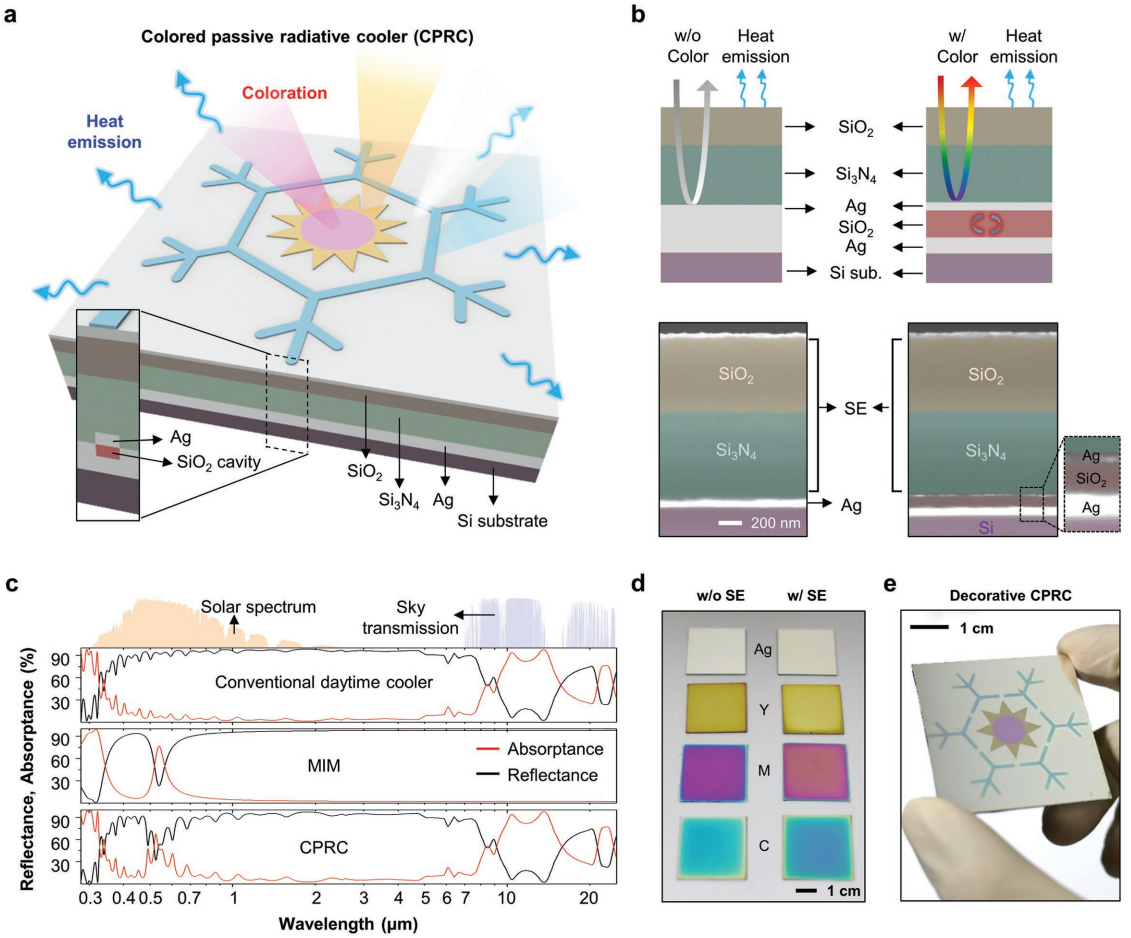

Figure 1. a) Schematic illustration of a colored passive radiative cooler (CPRC) exhibiting both silvery and colored areas, where the latter is a metal–insulator–metal (MIM; Ag-SiO_2-Ag) structure. A Si_3N_4/SiO_2 bilayer serves as the highly efficient thermal emitter, referred to as a selective emitter (SE). b) Cross-sectional schematic views (upper) and false-color scanning electron microscope (SEM) images (lower) of a conventional daytime radiative cooler (left) and CPRC (right). c) Reflectance and absorptance spectra from the visible to far-infrared wavelength range of a conventional daytime radiative cooler (upper), MIM structure (middle), and CPRC (lower). d) Photographs of bare Ag (top; left), conventional daytime cooler (top; right), MIMs (denoted Y, M, and C; left), and CPRCs (denoted Y, M, and C; right). e) Photograph of the decorative CPRC exhibiting color.

or subtractive color filters such as plasmonic nanopatterns (Figures S1 and S2, Supporting Information). The thin-layer geometry of the structure facilitated low-cost/large-area fabrication and the desired patterning with different colors. Moreover, such simple and thin layout secures a structural softness that enabled applications to a flexible device. Figure 1c exhibits the simulated reflectance/absorptance spectra of a conventional daytime radiative cooler, the MIM structure, and the CPRC, which is a combination of the two structures. As expected, the conventional daytime radiative cooler provides a high solar reflectance and efficient emission of thermal wavelengths in the atmospheric transparency window (Figure 1c, upper spectra). The MIM structure exhibits a reflection dip at a specific wavelength, which provides the tunable subtractive color by adjusting the cavity thickness (Figure 1c, middle spectra; Figure S3, Supporting Information). We note that the MIM structure perfectly blocks the thermal infrared wavelength and provides an isolation feature that creates independence between the SE and MIM structure. In other words, each structure does not hinder each characteristics, and thus the CPRC maintains pure colors corresponding to cyan, magenta, and yellow while effectively working as a radiative cooler (Figure 1c, bottom spectra). Figure 1d shows photographs of bare Ag film, conventional daytime cooler, MIMs, and CPRCs, demonstrating that there are no remarkable changes in the reflected colors of the MIM structures and CPRCs. The angular responses of MIM and CPRC exhibit the color resemblance of two structures at an oblique angle of incidence (AOI) as well (Figure S4, Supporting Information). Figure 1e exhibits a photograph of the decorative CPRC sample.

For a radiative sky cooling device to function in the daylight, it should simultaneously consider solar irradiation and atmospheric thermal radiation at the ambient air temperature, $T_{ambient}$. The cooling or heating capability of the passive radiative device is determined by the temperature of the cooler, T_{sample}, at a state of thermal equilibrium. For instance, the passive radiative device operates as a "cooler" when T_{sample} is lower than $T_{ambient}$, but acts as a "heater" in the opposite case. The relationship between the temperatures T_{sample} and $T_{ambient}$ is determined by the thermal equilibrium equation, given by[5]

$$P_{rad}\left(T_{sample}\right) - P_{Sun} - P_{atm}\left(T_{ambient}\right) + h_c\left(T_{sample} - T_{ambient}\right) = 0 \quad (1)$$

where $P_{rad}(T_{sample})$ is the radiation power of the sample at T_{sample}, P_{Sun} is the incident solar power absorbed by the structure, $P_{atm}(T_{ambient})$ is the absorbed power per unit area emanating from the atmosphere at $T_{ambient}$, and $h_c(T_{sample} - T_{ambient})$ is the nonradiative heat exchange term such as conductive and convective power, where h_c is nonradiative heat exchange coefficient. The detailed equations and calculation steps can be found in the Supporting Information.

In general, the appearance of color always accompanies the absorption of a particular spectrum in sunlight and P_{Sun} will thus be different depending on the desired colors in the structure, so the colors have a direct effect on the P_{Sun}. However, the combined term $P_{rad}(T_{sample}) - P_{atm}(T_{ambient})$ in Equation (1) is not generally ruled by solar absorption. With the large value of $(P_{rad} - P_{atm})$ added by introducing the SE, the CPRC can reach thermal equilibrium at lower temperatures than the MIM. **Figure 2**a shows the steady-state temperature and color difference, ΔE, of the CPRC as a function of the thickness of the top Ag layer and SiO_2 cavity for $h_c = 0$ (i.e., no conduction and convection). The ΔE is a mathematical description of the distance between two colors of CPRC and silver, demonstrating the vividness of the CPRC color compared with silver through quantified color examination. In all domain, the CPRC is heated to a maximum of only 6 K above ambient temperature while displaying the subtractive primaries of cyan, magenta, and yellow denoted at the SiO_2 cavity thicknesses of 90, 122, and 148 nm. The color representation method is descripted in the Supporting Information.

In short, the cooling and coloration depend on the thickness of the top Ag and the SiO_2 cavity, for example, the MIM with yellow has the minimum P_{Sun} because it has an absorption peak in short wavelength (i.e., weak solar intensity region). As the color of MIM shifts to magenta and cyan, the absorption peak of MIM shifts to near the peak of the solar irradiance, which increases P_{Sun} (Figure S5, Supporting Information). Figure 2b summarizes the correlation between the cooling and coloration as a function of the top Ag and SiO_2 cavity thicknesses. With a top Ag thickness of 20 nm the highest vivid color is observed but near-ambient heating, that is, maximum 6 K, is present (smaller region in Figure 2b). With the sacrifice of color purity, the cooling effect is further increased to allow subambient

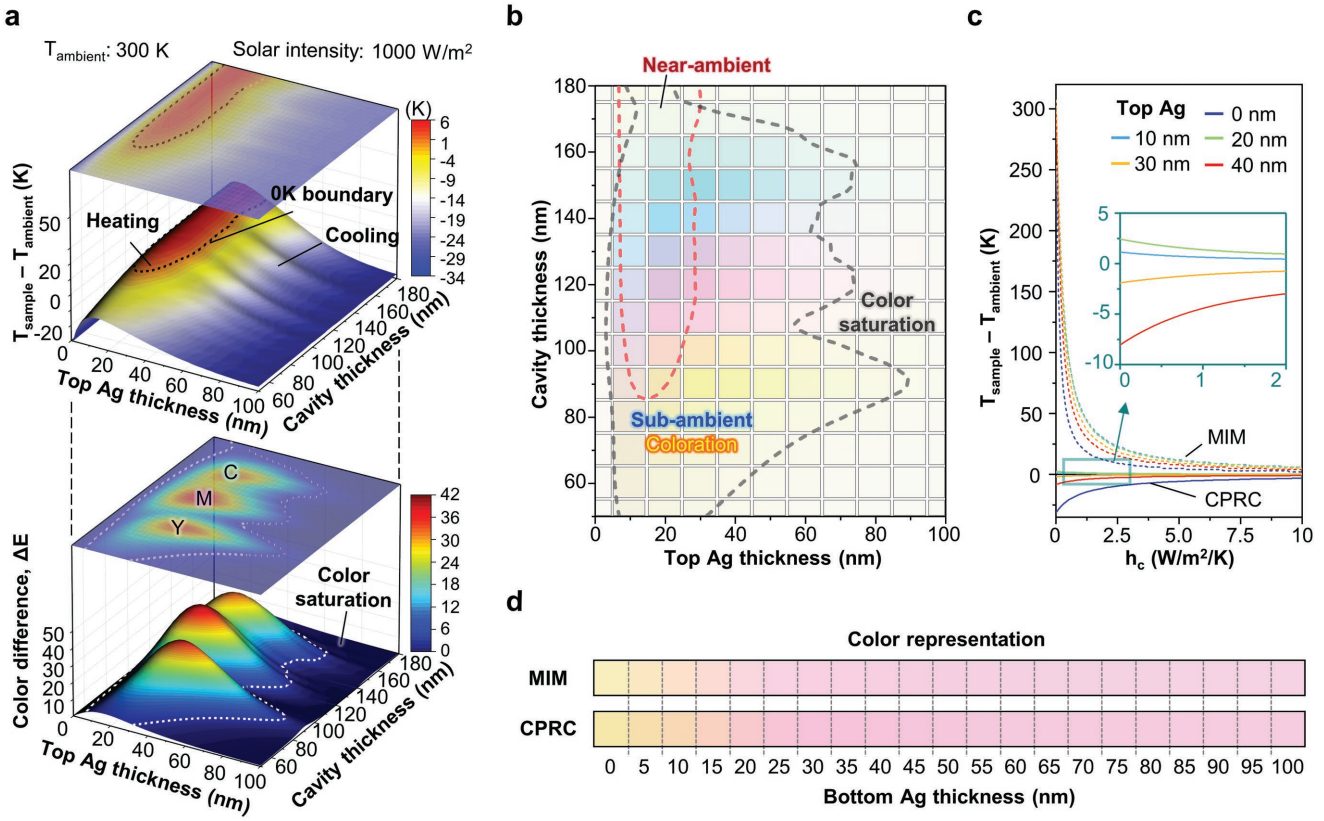

Figure 2. a) 3D contour plots for optimization of cooling capability and coloration of CPRC, which is a function of the thicknesses of the top Ag film and the SiO_2 cavity. (Top) Simulated temperature difference between the ambient air and the sample in the thermal equilibrium state. (Bottom) Color differences in a sample (where silver is the reference "color") based on simulated reflectance spectra. The secondary primary colors are indicated in the color difference map. b) Graph summarizing the information from (a) for the optimization of cooling and coloration with a color palette displaying the sample color as a function of the top Ag and SiO_2 cavity thicknesses. The inner red dashed region indicates where the colored passive radiative cooler (CPRC) is heated maximally to 6 K more than the ambient air with a solar intensity of 1000 W m^{-2}. The outer gray region indicates where the CPRC color saturates to silver. The CPRC design located between these two regions facilitates cooling and coloration simultaneously. c) Plot of $T_{sample} - T_{ambient}$ as a function of h_c for MIM and CPRC with a 100 nm thick bottom Ag and 120 nm thick SiO_2 cavity in different top Ag thicknesses. d) Color representations of MIM and CPRC as a function of bottom Ag thickness, with a 20 nm thick top Ag and a 120 nm thick SiO_2 cavity.

cooling, and the domain can thus be selected appropriately according to the application (larger region in Figure 2b). Each color is extinguished with top Ag layer thicknesses above 80 nm and the colored areas are not distinguishable from the bare Ag (Figure 2b), owing to the complete reduction of the reflectance dip with a thick top Ag layer (Figure S6a, Supporting Information). For the thickness variation of bottom Ag, the reflectance variation is nearly not found over 50 nm (Figure S6b, Supporting Information).

For highlighting the cooling effect of the SE, the $T_{sample} - T_{ambient}$ considering h_c is plotted for MIM and CPRC possessing 100 nm thick bottom Ag and 120 nm thick SiO_2 cavity with different top Ag thicknesses (Figure 2c). The $T_{sample} - T_{ambient}$ of the MIM dramatically increases to above 300K at $h_c = 0$ for all top Ag thicknesses although the temperature significantly drops as h_c increases. However, it still maintains a high temperature than the ambient air. On the contrary, the CPRC shows remarkable cooling characteristics regardless of h_c value. At thin top Ag (e.g., 10, 20 nm), the $T_{sample} - T_{ambient}$ is maximally sustained as above ≈2.5 °C than the ambient air. Thick top Ag layers (e.g., 30, 40 nm) present a subambient cooling performance, below 0 K of $T_{sample} - T_{ambient}$. Silvery surface (i.e., zero top Ag thickness) shows an exceptional cooling performance that is ≈–25 K of $T_{sample} - T_{ambient}$ at $h_c = 0$. In addition, the designed SE does not cause a noticeable color variation (Figure 2d, and Figure S7, Supporting Information). These theoretical analyses demonstrate that our SE not only lowers the temperature but also has color consistency of cooler, thereby CPRC exhibits outstanding cooling characteristics with the vivid colors despite zero nonradiative heat exchange.

For an efficient SE design, the geometrical parameters of the SE were optimized by comparing the averaged absorptance in the atmospheric transparency window region of 8–13 μm (Figure S8a,b, Supporting Information). **Figure 3**a shows the emissivity of the fabricated CPRC designed with these optimized characteristics, which is well-matched with the

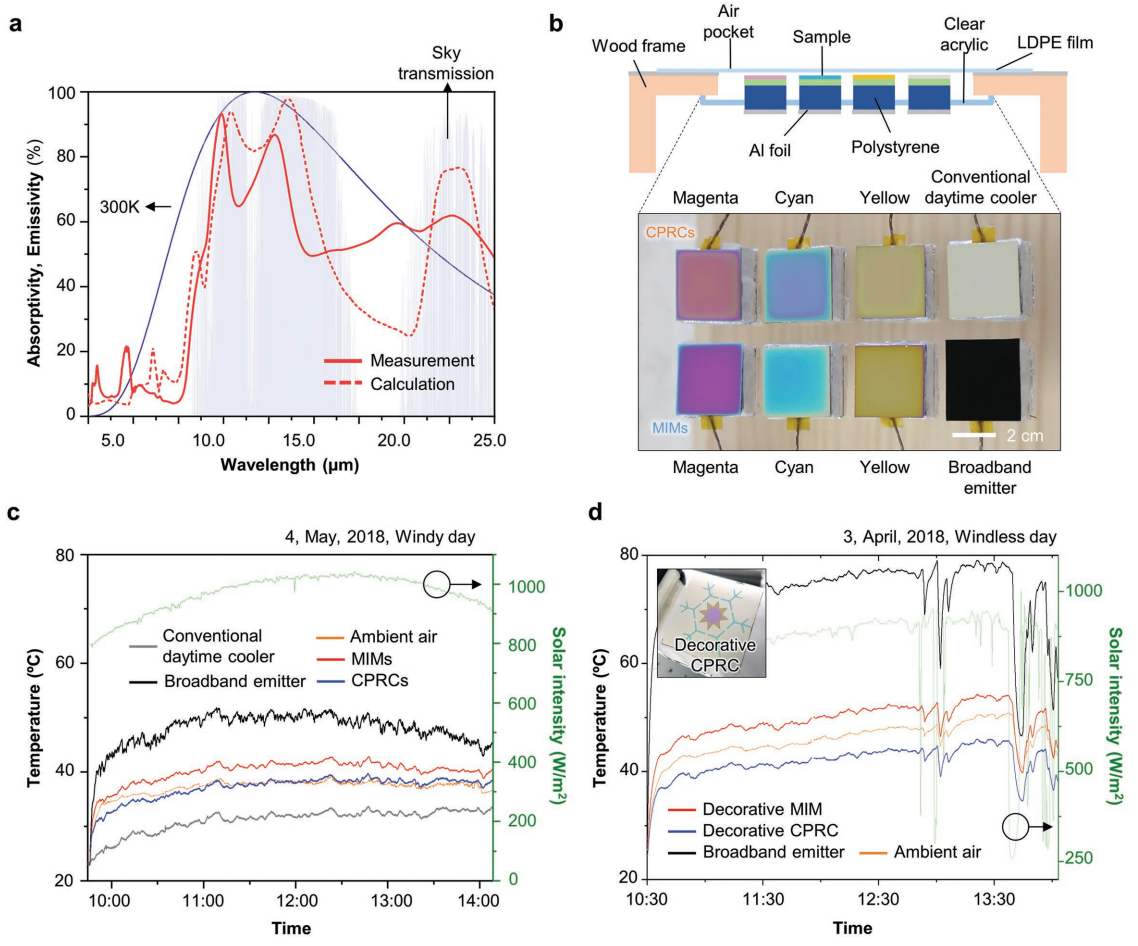

Figure 3. a) Absorptivity (or emissivity) features in the far-infrared wavelength region calculated for the designed structure (dashed line) and data measured from the structure (solid line). b) (Upper) Schematic illustration of measurement setup on rooftop. (Lower) Photograph of measured eight samples (i.e., conventional daytime cooler, broadband emitter, MIMs, and CPRCs with cyan, magenta, and yellow). c) Temperature measurements obtained on a rooftop from a commercial broadband emitter (black line), conventional daytime radiative cooler (gray line), MIM (red line), and CPRC (blue line) compared with the ambient air temperature (orange line) during the daytime. The logged temperatures of MIMs and CPRCs are averaged from three structures with different color structures. d) Temperature measurement of the decorative MIM (red line), the decorative CPRC (blue line), and broadband emitter (black line) during the daytime. The photograph displays the decorative CPRC. When the solar irradiation reduces owing to cloud screening, the temperatures of all samples immediately reduce.

theoretical calculation. The SE was designed to have peak emissivities at 10 and 12 μm, corresponding to the greatest sky transmission. Such two peak points in the designed SE sustain a high emissivity in the atmospheric window region to the AOI of 80°. The angular emissivity is followed by Lambertian profile in all sample temperatures (Figure S8c,d, Supporting Information). Further, the transparency characteristics of the SiO_2 and Si_3N_4 prevent solar absorption in the visible range (Figure S9, Supporting Information). The detailed optimization process for the SE is explained in the Supporting Information. The measurement setup was designed to reduce both convection and conduction to the radiative cooler under peak solar irradiation by sealing it with a low-density polyethylene film functioning as a wind shield (Figure 2b, top). Aluminum foil covered the wooden frame, which reflected the sunlight and thus prevented heating of the wooden frame. Our samples were placed on a polystyrene block that was also wrapped by Al foil, and the polystyrene block was supported by a clear acrylic box. The overall design of this setup was obtained from the work published in ref. [5]. The photographs show a broadband emitter, Ag film with the SE (i.e., conventional daytime cooler), MIMs, and CPRCs (Figure 2b; bottom). To enable exposure of our samples during an extended period of the day, the experiment setup was placed on a supporter tilted 30° toward the south, and the test was conducted on a rooftop of a building at the Gwangju Institute of Science and Technology (GIST), Gwangju, South Korea. The detailed approaches for temperature and solar irradiance recording are descripted in the Supporting Information.

At first, the daytime cooling performance of CPRCs with the subtractive primaries is investigated on a clear spring day by exposing to the sun. The temperature measurements of the eight samples exposed to the sky are plotted in Figure 3c. In the case of MIMs and CPRCs, the logged temperatures for each separate color are averaged to plot the value as a function of time, while all temperature data for each individual color are given in Figure S10 (Supporting Information). After exposure to sky, the temperatures of the samples immediately increase except for the conventional daytime cooler. The temperature of the conventional daytime cooler drops below the ambient air temperature 5.9 °C on average and 9.3 °C maximally. Contrarily, the broadband emitter heats up remarkably to 10.5 °C more than the ambient air. The average temperature of the MIMs is maximally 4.5 °C higher than that of the ambient air, while the CPRCs maintain a near-ambient temperature (<0.05 °C below ambient on average) under strong solar irradiation. The experiment was sustained for over 4 h, during which period the incident solar power to the samples exceeded 800 W m^{-2}. This experimental data demonstrate that CPRCs can maintain near-ambient temperatures even while displaying vivid colors. In addition to daytime cooling, the night-time cooling results demonstrate that CPRCs have a feature comparatively cooler than a commercial broadband emitter (Figure S11, Supporting Information). Typically, roof and building materials have high-absorption characteristics and heat significantly under direct solar irradiation. Therefore, the CPRCs can be used as an exterior material that is relatively cooled.

Figure 3d highlights the subambient cooling of the decorative CPRC with no additional cooling strategies such as water-based or air-based convection/conduction active systems. The decorative CPRC is capable of subambient cooling featuring a highly reflective background (i.e., silver), which boosts the net cooling capacity. Quantitative measurements were obtained of the temperatures of the broadband emitter, decorative MIM (i.e., without SE), and the decorative CPRC, which were acquired continuously for 3.5 h. The broadband emitter reaches 70 °C a few minutes after being exposed to the sun. The decorative MIM heats up to 3.5 °C above the ambient temperature, whereas the CPRC maintains a temperature that is on average 3.9 °C below the ambient air at all times. When the clouds screen the sunlight the temperatures rapidly drop, but the CPRC still exhibits the lowest temperature among the three structures. In addition to daytime cooling, the CPRC also exhibits a remarkable performance for night-time cooling (Figure S12, Supporting Information).

In recent times, the size of modern electronic devices such as portable and wearable devices have decreased significantly while their power density has increased, thus raising serious concerns about exponential self-heating.[27,28] In these hand-held devices, sufficient cooling for a long operating time is imperative because it maximizes the battery efficiency. For this purpose, a passive cooling approach is a promising option for addressing the self-heating issue of these modern electronics.[22] Further, multifunctional wearable devices require effective heat dissipation to prevent thermal damage to biological tissue[29,30] and deterioration in functionality.[31–34]

Figure 4a schematically illustrates a flexible radiative cooling material (fRCM) to address the thermal issues in modern small electronics. For compatibility with wearable devices, common Al foil was used as a substrate owing to its mechanical softness, low cost, and an excellent solar reflector feature (Figures S13 and S14, Supporting Information). The pristine states of fRCM are shown in Figure S15 (Supporting Information). After depositing the MIM and SE on the Al foil, polydimethylsiloxane (PDMS) was used as an encapsulation layer for protection and to assist in radiative heat emission owing to its prominent emissivity in the thermal infrared regions (Figure S16, Supporting Information). Owing to the thin film structures of the MIM and SE, the combined layers exhibit a softness that allows for bending. The heating device used in this study was fabricated on a polyimide film 125 μm thick with serpentine electrode, which is the representative method used to establish flexibility and stretchability in the field of flexible/stretchable electronics.[35,36]

The surface temperature of small electronics should be maintained below a certain threshold (i.e., 45 and 41 °C for plastic and aluminum enclosures, respectively) to prevent user discomfort.[37] To evaluate the surface temperature reduction capability of the fRCM, the surface temperatures of the heating device were observed in three states: (i) bare heater, (ii) covered by Al foil coated with PDMS, and (iii) covered by the fRCM, by using a thermal imaging camera (Figure 4b). To ensure conformal contact of the covering materials with the heating device, a PDMS layer ≈1 mm thick was laminated onto the heating device. To measure the exact surface temperature of the heating device, an attachable thermocouple is utilized (Figure S17, Supporting Information). The maximum surface temperatures were increased by raising the supplied current to the heating device, varying as 0.35 and 0.45 A, in all the

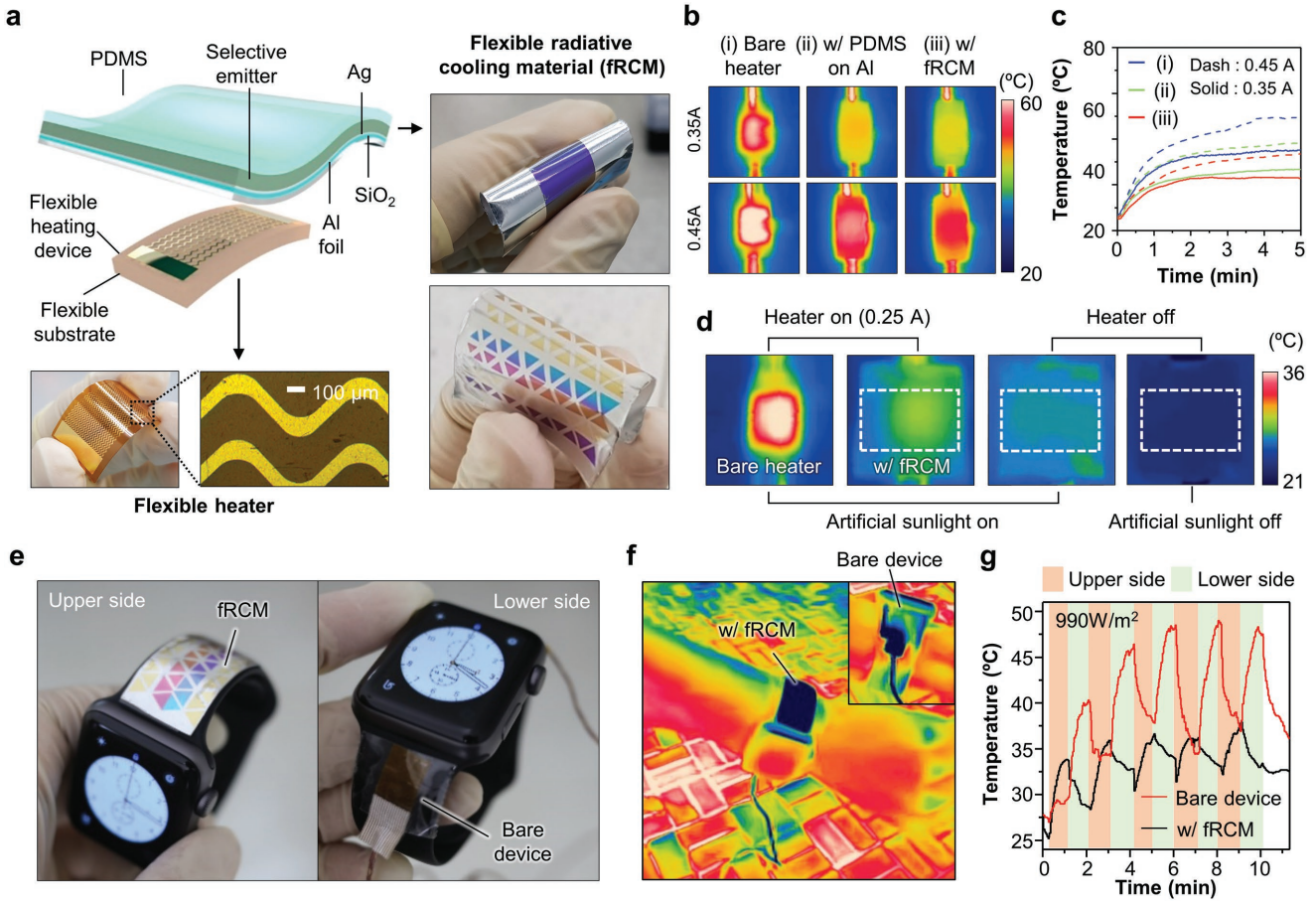

Figure 4. a) Schematic illustration of the flexible radiative cooling material (fRCM). The photographs of (right) fRCMs and (bottom) flexible/stretchable heating device. b) Thermal images of (left) the flexible heater uncovered, (center) covered by the Al foil coated with PDMS, and (right) covered by the fRCM. The applied currents are different at upper and bottom rows (i.e., upper row: 0.35 A, bottom row: 0.45 A). c) Measured temperatures of the flexible heaters: (i) bare heater, (ii) covering by Al coated with PDMS, and (iii) the fRCM. Dashed and solid lines indicate the applied currents such as 0.45 and 0.35 A. d) Thermal radiation test of the fRCM on the heater when exposed to artificial solar irradiation, where the white dashed box indicates the fRCM colored area shown in the left image in (b) and in Figure S14a (Supporting Information). e) Photographs of a practical wearable device covered (left) and uncovered (right) by an attached fRCM. f) Thermal image of the practical wearable device areas covered and uncovered (inset image) by fRCM. The temperature difference is observed due to fRCM under strong solar irradiation at mid-day, 990 W m^{-2}. g) Temperature data from the wearable device in areas uncovered (red data) and covered (black data) by the fRCM.

samples (Figure 4c). The resulting temperatures were measured at the supplied currents of 0.35 and 0.45 A as follows: (1) bare heater registered maximally 55.3 and 69.0 °C; (2) heating device with Al foil coated with PDMS registered maximally 46.7 and 58.1 °C; and (3) heating device with the fRCM registered 42.9 and 53.4 °C, respectively. The detailed measurement setup for thermal imaging and description are given in the Experimental Section and Figure S18 (Supporting Information). In general, to prevent thermal damage to epidermal tissues, wearable devices should not exceed the critical surface temperatures, where the first-degree burns and the third-degree burns are obtained at 54 and 60 °C, respectively.[38] In this context, covering the heating device with the fRCM remarkably lowers the high surface temperatures of 55.3 and 69.0 °C (i.e., 0.35 and 0.45 A), which would cause epidermal damage, to sufficiently low temperatures of 42.9 and 53.4 °C. Therefore, this result demonstrates the ability of the fRCM to reduce the surface temperature of small electronics, thereby preventing thermal damage to the skin and enhancing the battery efficiency of portable and wearable devices.

The electronics of wearable devices can be regularly exposed to the sun, and thus the joule heating by device operation (i.e., conduction) must be considered in conjunction with the effect of solar irradiation (i.e., radiation). In particular, because the fRCM possessed a specific colored area that highly absorbed sunlight, solar irradiation must be considered. Figure 4d exhibits the surface temperature variation of the operating device under solar irradiation in the laboratory, where the white dashed box indicates the colored area on the fRCM (Figure 4a, and Figure S15a, Supporting Information). The maximum temperature of the bare heating device under artificial sunlight was 37.3 °C, which dropped to 27.7 °C when the fRCM was placed on the heating device. When the heating device was turned off, the surface temperature in the colored area was slightly higher (i.e., 0.2 °C higher) than the silvery area (25.5 °C) owing to artificial solar irradiation. After screening the artificial sunlight to

remove heat sources, the overall surface temperature reached 22.2 °C. This result demonstrates that an fRCM with colored areas can cool the surface temperature of a device sufficiently when considering both conduction and solar irradiation.

Figure 4e–g highlights the effectiveness of the fRCM thermal management by covering a wearable device, that is, a "smart" watch (Apple watch 3; Apple, USA). The fRCM was attached to the upper side of the device while the lower side of the device was uncovered (Figure 4e). The thermal image demonstrates the temperature difference existing between the fRCM-covered (Figure 4f) and fRCM-uncovered sides of the device (Figure 4f, inset) when each side is exposed to the sun. The temperature data of this in Figure 4g demonstrates this cooling effect of the fRCM. When the upper (i.e., covered) side of the device was initially exposed to the sunlight, the temperature increased in the upper side than the lower (i.e., uncovered) side. Once the device was flipped so that the uncovered side was directly exposed to the sun, the temperature in the uncovered side increase, whereas the temperature in the covered side decreased to ≈28 °C. With the repetition of device flip, the temperature in the uncovered side was increased and kept over 35–48 °C. Contrarily, the covered side maintained a relative low temperature, 30–37 °C, owing to minimal solar absorption and radiative cooling. Also, fRCM functions when directly contacting to the skin in large area (Figure S19, Supporting Information). These experimental results prove that the passive radiation-based cooling strategy is effective to suppress the heating of small electronics under solar irradiation.

In summary, we have presented a photonic approach to fabricate a CPRC for aesthetic purposes by embedding a subtractive color film comprising a MIM structure beneath a SE layer composed of Si_3N_4 and SiO_2. The spectral, color, and thermal analyses of this CPRC provided evidence of near-ambient and even subambient cooling. Based on this design rule, CPRCs exhibiting the subtractive primary colors (i.e., cyan, magenta, and yellow) were fabricated and tested under solar irradiation to estimate their applicability as a radiative cooling device for daytime cooling. In addition to monochrome samples, a multicolor CPRC exhibiting a silvery background to boost the net cooling efficiency was tested in the daytime. This CPRC demonstrated an outstanding cooling performance that exhibited subambient cooling for 24 h. This scheme was also compatible with small modern electronics such as wearable devices, after creating a flexible CPRC by depositing the MIM and SE structures on flexible Al foil. This flexible radiative cooling material could lower the surface temperature of the device in its operation state, thereby enabling increased battery efficiency and preventing thermal damage to the epidermis. Collectively, these features suggest the advantage of addressing the installation space limitation of conventional passive cooling while enhancing the net cooling capacity, and of practical application with temperature-sensitive, high-power electronics and wearable devices.

Experimental Section

The experimental details, including structure designs, fabrication, and characterization, are provided in the Supporting Information.

Supporting Information

Supporting Information is available from the Wiley Online Library or from the author.

Acknowledgements

This research was supported by the National Research Foundation of Korea (NRF) (NRF-2017M3D1A1039288, NRF-2017R1D1A1B03028055). This work was also supported by GIST Research Institute (GRI) grant funded by the GIST in 2018. G.J.L. acknowledges the support from the NRF (NRF-2017H1A2A1042138).

Conflict of Interest

The authors declare no conflict of interest.

Keywords

coloration, colored radiative cooler, flexible radiative cooler, passive radiative cooling

Received: May 30, 2018
Revised: July 19, 2018
Published online: August 27, 2018

[1] E. A. Goldstein, A. P. Raman, S. Fan, *Nat. Energy* **2017**, *2*, 17143.
[2] N. Fernandez, W. Wang, K. J. Alvine, S. Katipamula, *Energy Savings Potential of Radiative Cooling Technologies Technical Report*, *PNNL24904*, Pacific Northwest National Laboratory, Richland, WA **2015**.
[3] M. Deru, K. Field, D. Studer, K. Benne, B. Griffith, P. Torcellini, B. Liu, M. Halverson, D. Winiarski, M. Rosenberg, M. Yazdanian, J. Huang, D. Crawley, *U.S. Department of Energy Commercial Reference Building Models of the National Building Stock Technical Report*, *NREL/TP-5500-46861*, National Renewable Energy Laboratory, Golden, CO **2011**.
[4] M. Issac, D. P. van Vuuren, *Energy Policy* **2009**, *37*, 507.
[5] A. P. Raman, M. A. Anoma, L. Zhu, E. Rephaeli, S. Fan, *Nature* **2014**, *515*, 540.
[6] Y. Zhai, Y. Ma, S. N. David, D. Zhao, R. Lou, G. Tan, R. Yang, X. Yin, *Science* **2017**, *355*, 1062.
[7] S. H. Choi, S.-W. Kim, Z. Ku, M. A. Visbal-Onufrak, S.-R. Kim, K.-H. Choi, H. Ko, W. Choi, A. M. Urbas, T.-W. Goo, Y. L. Kim, *Nat. Commun.* **2018**, *9*, 452.
[8] S. Atiganyanun, J. B. Plumley, S. J. Han, K. Hsu, J. Cytrynbaum, T. L. Peng, S. M. Han, S. E. Han, *ACS Photonics* **2018**, *5*, 1181.
[9] J.-I. Kou, Z. Jurado, Z. Chen, S. Fan, A. J. Minnich, *ACS Photonics* **2017**, *4*, 626.
[10] A. R. Gentle, G. B. Smith, *Adv. Sci.* **2015**, *2*, 1500119.
[11] M. M. Hossain, B. Jia, M. Gu, *Adv. Opt. Mater.* **2016**, *3*, 1047.
[12] E. Rephaeli, A. Raman, S. Fan, *Nano Lett.* **2013**, *13*, 1457.
[13] A. R. Gentle, G. B. Smith, *Nano Lett.* **2010**, *10*, 373.
[14] M. Sameti, A. Kasaeian, *Build. Simul.* **2015**, *8*, 239.
[15] W. Li, Y. Shi, K. Chen, L. Zhu, S. Fan, *ACS Photonics* **2017**, *4*, 774.
[16] L. Zhu, A. P. Raman, K. X. Wang, M. A. Anoma, S. Fan, *Optica* **2014**, *1*, 32.
[17] L. Zhu, A. P. Raman, S. Fan, *Proc. Natl. Acad. Sci. USA* **2015**, *112*, 12282.
[18] E. Rephaeli, S. Fan, *Opt. Express* **2009**, *17*, 15145.
[19] E. Sakr, P. Bermel, *Opt. Express* **2017**, *25*, A880.

[20] Y. Nam, Y. X. Yang, A. Lenert, P. Bermel, I. Celanovic, M. Soljacic, E. N. Wang, *Sol. Energy Mater. Sol. Cells* **2014**, *122*, 287.
[21] S. J. Byrnes, R. Blanchard, F. Capasso, *Proc. Natl. Acad. Sci. USA* **2014**, *111*, 3927.
[22] X. Sun, Y. Sun, Z. Zhou, M. A. Alam, P. Bermel, *Nanophotonics* **2017**, *6*, 997.
[23] Comparing tablet natural convection cooling efficiency, https://www.mentor.com/products/mechanical/engineering-edge/volume3/issue1/comparing-natural-convection-cooling-efficiency (accessed: May 2018).
[24] E. Yu, Y. K. Joshi, *J. Heat Transfer* **1999**, *121*, 1002.
[25] K. D. Vogeleer, G. Memmi, P. Jouvelot, F. Coelho, **2014**, arXiv:1410.0628.
[26] L. Zhu, A. Raman, S. Fan, *Appl. Phys. Lett.* **2013**, *103*, 223902.
[27] K. Maize, S. R. Das, S. Sadeque, A. M. S. Mohammed, A. Shakouri, D. B. Janes, M. A. Alam, *Appl. Phys. Lett.* **2015**, *106*, 143104.
[28] M. A. Wahab, S. Shin, M. A. Alam, presented at *2016 IEEE Int. Reliability Physics Symp. (IRPS)*, Pasadena, CA, April **2016**.
[29] T.-I. Kim, J. G. McCall, Y. H. Jung, X. Huang, E. R. Siuda, Y. Li, Y. M. Song, H. A. Pao, C. Lu, S. D. Lee, I. S. Song, G. C. Shin, M. P. Tan, Y. Huang, J. A. Rogers, *Science* **2013**, *340*, 211.
[30] F. Xu, P. F. Wang, M. Lin, T. J. Lu, E. Y. K. Ng, *J. Mech. Med. Biol.* **2010**, *10*, 373.
[31] S. W. Chae, K. C. Kim, D. H. Kim, T. G. Kim, S. K. Yoon, B. W. Oh, D. S. Kim, H. K. Kim, Y. M. Sung, *Appl. Phys. Lett.* **2007**, *90*, 181101.
[32] Q. Zhou, M. O. Manasreh, *Appl. Phys. Lett.* **2001**, *79*, 2901.
[33] G. Maneghesso, M. Meneghini, E. Zanoni, *J. Phys. D: Appl. Phys.* **2010**, *43*, 354007.
[34] T.-I. Kim, S. H. Lee, Y. Li, Y. Shi, G. Shin, S. D. Lee, Y. Huang, J. A. Rogers, J. S. Yu, *Appl. Phys. Lett.* **2014**, *104*, 051901.
[35] D.-H. Kim, N. Lu, R. Ma, Y.-S. Kim, R.-H. Kim, S. Wang, J. Wu, S. M. Won, A. Islam, K. J. Yu, T.-I. Kim, R. Chowdhury, M. Ying, L. Xu, M. Li, H.-J. Chung, H. Keum, M. McCormick, P. Liu, Y.-W. Zhang, F. G. Omenetto, Y. Huang, T. coleman, J. A. Rogers, *Science* **2011**, *333*, 838.
[36] Y. M. Song, Y. Xie, V. Malyarchuk, J. Xiao, I. Jung, K.-J. Choi, Z. Liu, H. Park, C. Lu, R.-H. Kim, R. Li, K. B. Crozier, Y. Huang, J. A. Rogers, *Nature* **2013**, *497*, 95.
[37] M. K. Berhe, presented at *ASME 2007 InterPACK Conf.*, Vancouver, BC, Canada, July **2007**.
[38] M. G. Jeschke, L.-P. Kamolz, S. Shahrokhi, *Burn Care and Treatment*, Springer-Verlag Wien, Vienna, Austria **2013**.